Glass relaxation and hysteresis of the glass transition by molecular dynamics simulations

Zegao Liu,[1] Yushu Hu,[1] Xin Li,[1] Weiying Song,[1] Sushmit Goyal,[2] Matthieu Micoulaut,[3,*] and Mathieu Bauchy[1]

[1]*Physics of AmoRphous and Inorganic Solids Laboratory (PARISlab), Department of Civil and Environmental Engineering, University of California, Los Angeles, California 90095, USA*

[2]*Science and Technology Division, Corning Incorporated, Corning, New York 14831, USA*

[3]*Physique Théorique de la Matière Condensée, Sorbonne Université, Paris, 75252, France*

(Received 19 June 2018; revised manuscript received 24 August 2018; published 21 September 2018)

As out-of-equilibrium materials, glasses continually tend to relax toward the metastable supercooled liquid state. Glass relaxation can result in a nonreversible glass transition upon a cooling/reheating cycle. Here, based on molecular dynamics simulations, we present a methodology combining thermal cycles and inherent configuration analysis to investigate the features of relaxation and glass transition reversibility. By considering three archetypical silicate glasses, viz., silica, sodium silicate, and calcium aluminosilicate, we show that, for all the glasses considered herein, the enthalpy relaxation can be well described by mode-coupling theory. Further, we demonstrate the existence of a decoupling between enthalpy and volume relaxation. Finally, we show that enthalpy relaxation results in a nonreversible glass transition—the degree of nonreversibility being strongly system-specific.

DOI: 10.1103/PhysRevB.98.104205

I. INTRODUCTION

The crystallization of a liquid can be avoided if cooled fast enough [1]. At temperatures lower than the melting temperature, supercooled liquids are a thermodynamic metastable state [2]. With decreasing temperature, the viscosity η and the relaxation time to equilibrium $\boldsymbol{\tau}$ tend to dramatically increase. At some reference temperature defined in the literature as the glass transition temperature T_g, η reaches the value 10^{12} Pa · s, which roughly corresponds to a relaxation time of 100 s [3]. At lower temperatures, the very viscous liquids exhibit all the typical macroscopic properties of a solid and these properties now depend on the waiting time before the realized measurement [4,5]. This simply signals that glasses are out-of-equilibrium materials and their properties evolve slowly with time [6].

A conventional means to measure such effects is to rely on calorimetric methods. As the equilibration cannot proceed further upon cooling (because of the rapid increase of the relaxation time with decreasing temperature) the enthalpy curve or the volume curve deviates from the high-temperature equilibrium line at the fictive temperature T_f—this temperature T_f depending explicitly on the cooling rate [3]. As a result, the specific heat (C_p) displays an abrupt decrease across T_f, which signals that the translational and rotational degrees of freedom of the glass are now frozen [7]. However, even in the resulting glassy state, the material continues to relax toward lower enthalpies, but over timescales that exceed the laboratory timescale by several orders of magnitude [2]. Upon reheating, the behavior of the specific heat is markedly different from the cooling curve and a hysteresis can be evidenced. The extent of hysteresis depends on the heating rate, the temperature at which the glass has relaxed, and the waiting time before which the calorimetric experiment is performed [3]. This heating experiment, furthermore, leads to a heat capacity overshoot at the glass transition and this endotherm signals that relaxation has taken place due to their intrinsic out-of-equilibrium nature of the glassy state [8]. Relaxation effects are technologically important as they can cause undesirable variations in the dimensions of glassy substrates for displays application during processing, which can eventually result in some pixel misalignment [9]. In select situations and applications, one is targeting a reduced relaxation tendency that can induce a minimal hysteresis in enthalpy or molar volume. However, it is not clear which physical and chemical properties drive such "ideal" glasses. Yet, it has recently been found that such hysteresis curves are minimized when the liquid reaches a critical mechanical state with an optimal reduction of both low-frequency relaxation and bond energy minima of the potential-energy landscape [10,11].

Molecular dynamics (MD) simulations can shed some light on such phenomena by relating the thermal or energy behavior with different materials properties such as structure and mechanical properties [12]. In this respect, the relaxation of glass has been related to the effects of pressure [10], composition [13], coordination numbers [14], and other factors [15]. However, a well-known shortcoming of MD simulations is their timescale, which can only extend to the μs range—so that the typical timescales associated with glassy relaxation at T_g (seconds) are out of reach [16]. Correspondingly, the viscosity range that can be investigated is of about tens or hundreds of Pa·s only. However, one has to keep in mind that all the salient features associated with the experimental onset of an out-of-equilibrium dynamics can be recovered from simulations—although the associated timescale is shifted with respect to experiments [17,18]. This timescale difference leads to an overestimation of the glass fictive temperature,

*mmi@lptl.jussieu.fr

which is usually larger in simulations by several hundred of degrees when compared to the experimental counterpart due to much larger cooling rates (on the order of a few K/ps). Such large values of cooling rates are actually fairly compatible with those experienced experimentally in very small samples, wherein surface is large as compared to volume—so that surface energy dissipation can occur fast [19]. Numerical studies have, furthermore, revealed that the relaxation time and the viscosity can be accurately investigated from simulations and associated results compare favorably with experimental data of high-temperature liquids—while being sometimes extrapolated with confidence to lower temperatures [20]. Similarly, the freezing of density-density correlations in Fourier space at low temperature can also be recovered (i.e., the β-relaxation plateau associated with the cagelike dynamics of supercooled liquids) and the behavior of heat capacities across the glass transition region is rather well-described [15]. Having such intrinsic limitations at hand, MD simulations represent, still, a powerful technique able to substantiate the notion of glass reversibility and connect the behavior with materials properties at large.

In the present paper, we address this issue of glass reversibility by focusing on numerical cooling/heating cycles across the glass transition. We perform MD simulations of three archetypal silicate glasses: (i) silica, SiO_2, the base system for all silicate glasses [3], (ii) sodium silicate, $(Na_2O)_{30}(SiO_2)_{70}$, a model for all alkali silicate glasses used for ion-exchange treatments [21,22], and (iii) calcium aluminosilicate, $(CaO)_{24}(Al_2O_3)_{24}(SiO_2)_{52}$, a model for all alkali-free display glasses used for liquid-crystal display (LCD) and organic light-emitting diode (OLED) glass substrates [9]. A methodology combining thermal cycles and inherent configuration analysis is introduced and serves for the characterization of the features of relaxation in relationship with glass transition reversibility. We first show that our simulations reproduce the generic features of the glass transition. Following this, we find that, for all the considered glasses, enthalpy relaxation follows a power-law dependence as a function of the cooling rate—in agreement with an earlier prediction of mode-coupling theory. This permits us to determine the increase of enthalpy at 0 K due to a finite cooling rate with respect to that which would be achieved for a (fictitious) zero-cooling rate. Further, we demonstrate that enthalpy and volume relaxation are decoupled from each other. Then, we perform cooling/heating cycles in order to measure the degree of relaxation visible from the extent of the induced hysteresis curve. We find that both the enthalpy relaxation and the range of temperature over which it occurs are strongly system-specific, although some general conclusions can be drawn.

II. SIMULATION DETAILS

A. Preparation of the melts

To establish our conclusions, three archetypal silicate glasses are simulated with MD: (i) silica (S), SiO_2; (ii) sodium silicate (NS), $(Na_2O)_{30}(SiO_2)_{70}$; and (iii) calcium aluminosilicate (CAS), $(CaO)_{24}(Al_2O_3)_{24}(SiO_2)_{52}$. All simulations were carried out with the LAMMPS package [23]. The initial liquid configurations were generated by (i) randomly placing around 3000 atoms in a cubic simulations box while ensuring the absence of any unrealistic overlap, (ii) melting the system at 4000 K for 100 ps (NVT ensemble) to ensure the loss of the memory of the initial configuration, and (iii) relaxing the system at 4000 K under zero pressure (NPT ensemble) for 100 ps. For all systems, a time step of 1 fs is used, while temperature and pressure are imposed via a Nosé-Hoover thermostat and barostat, using some damping parameter of 100 and 1000 fs, respectively [24,25].

Since empirical force fields have a limited transferability over varying configurations, a specific interatomic potential was chosen for each system. However, although each potential relies on a system-specific parametrization, they all rely on fixed partial charges and a simple two-body Buckingham potential formulation. In all cases, the Coulombic interactions were evaluated with the Ewald summation method—with a convergence criterion factor of 10^{-5}. First, the well-established potential developed by van Beest, Kramer, and van Santen (BKS) was used to simulate silica [26]. The cutoff was fixed at 5.5 and 10 Å for the short-range and Coulombic interactions, respectively—as this specific choice has shown to yield an improved description of the glass density [27]. The BKS potential has shown to offer a very good description of the structural, dynamical, and mechanical properties of silica [27–30]. Second, we relied on the potential parametrized by Teter to simulate the NS glass [31]. The cutoff was fixed at 8 and 12 Å for the short-range and Coulombic interactions, respectively. This potential has been extensively studied and has been found to offer an excellent description of the structural, dynamical, vibrational, and thermodynamical properties of NS glasses [10,17,29,31–39]. Finally, the potential developed by Jakse and co-workers was used to simulate the CAS glass [40,41]. The cutoff was fixed at 8 and 12 Å for the short-range and Coulombic interactions, respectively. This potential has shown to yield an excellent description of the structural, mechanical, and vibrational properties of CAS glasses [29,42].

B. Thermal cycling methodology

To assess the degree of reversibility of the glass transition of these systems, all three glasses were subjected to a thermal cycle, details of which are as follows [11,43]. Starting from well-relaxed liquid configurations, the systems were cooled and subsequently reheated at varying cooling/heating rates (from 100 to 0.1 K/ps, with temperatures steps of 100 K) in the NPT ensemble and zero pressure. To filter out any thermal effect, 16 independent configurations were extracted every 1 ps at the end of each temperature step. All configurations were then subjected to an energy minimization in order to compute the enthalpy of their inherent configuration (local ground-state enthalpy) [17,44]. All the results presented below are averaged over these 16 configurations. We ensured that the results of the thermal cycling simulations are not affected by any spurious effect of the thermostat and barostat (see Supplemental Material) [45].

III. RESULTS AND DISCUSSION

A. Features of the glass transition

Figure 1 represents the local ground-state enthalpy H as a function of the temperature T (i.e., the enthalpy of the inherent

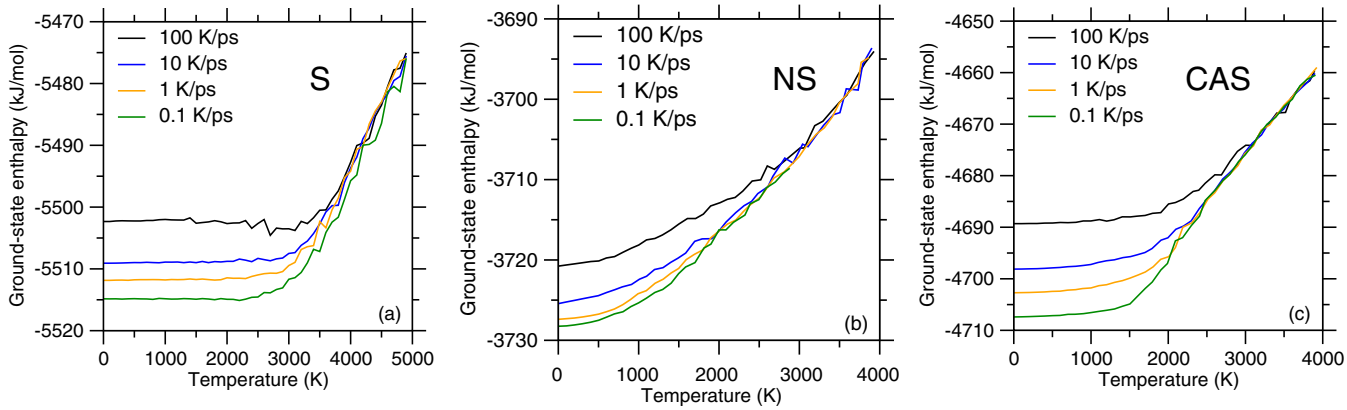

FIG. 1. Local ground-state enthalpy $H(T)$ (i.e., enthalpy of the inherent configuration) as a function of temperature T under select cooling rates for (a) silica (S), (b) sodium silicate (NS), and (c) calcium aluminosilicate (CAS). Note that each panel has a different y axis.

configuration for each temperature). For all systems, H decreases monotonically with decreasing temperature. We note that S has the lowest ground-state enthalpy, which is found between -5515 and -5500 kJ/mol for the studied cooling rates, whereas NS has the highest ground-state enthalpy. Since the enthalpy also reflects at the atomic scale a bond energy density, this result agrees with the fact that S is more polymerized and NS is less polymerized due to the formation of nonbridging oxygen species caused by sodium atoms [31].

At a certain temperature (the fictive temperature [46], called T_f hereafter), the salient features of the glass transition are recovered and a break in the slope of $H(T)$ is observed for the three glasses. This is an indication that the system can no longer equilibrate over the imposed computational timescale. We, furthermore, note that S and CAS glasses have a sharper transition [given the obvious larger changes in $dH(T)/dT$ across the glass transition], whereas NS exhibits a more gradual transition. When the position of the break in slope is considered (i.e., the fictive temperature), we find that $T_f(S) > T_f(CAS) > T_f(NS)$, in agreement with experimental results [47–49]. Further, the fictive temperature decreases with decreasing cooling rate for the three glasses [46]. Overall, the simulations reproduce the generic features of the effect of the cooling rate on the enthalpy across the glass transition.

For S and CAS glass, the local ground-state enthalpy $H(T)$ shows a plateau at low temperature and $H(T)$ barely depends on temperature. This signals a weak temperature dependence of the specific heat. The zero-temperature ground-state enthalpy decreases monotonically with decreasing cooling rate for the three glasses, which is in line with experimental results [10,50] and is simply the indication that the glasses achieved with a lower cooling rate have relaxed toward lower energy values. Conversely, there is no such plateau for the NS glass and a continuous decrease upon decreasing temperature is observed. The suggests that, unlike S and CAS glasses, NS exhibits some more pronounced structural relaxation that leads to a larger enthalpic evolution below T_f. This effect likely results from the higher mobility of the Na atoms, even at low temperature [51]. For instance, we find that, at 800 K (i.e., below T_f), the mobility of the Na atoms is nearly two orders of magnitude higher than that of all the other species (including Ca atoms; see Supplemental Material) [45].

We next focus on the variations in the molar volume V_m (Fig. 2). For the NS and CAS glasses, the molar volume decreases monotonically with decreasing temperature [52] and a break of slope is also observed around the fictive temperature—although the break of slope is not as sharp as that observed in the case of the local ground-state enthalpy. Note that the break of slope leads to a change in the thermal expansion coefficient at the glass transition [53]. For silica, one notices that the molar volume exhibits an anomalous behavior, that is, a minimum at around 5000 K—in agreement

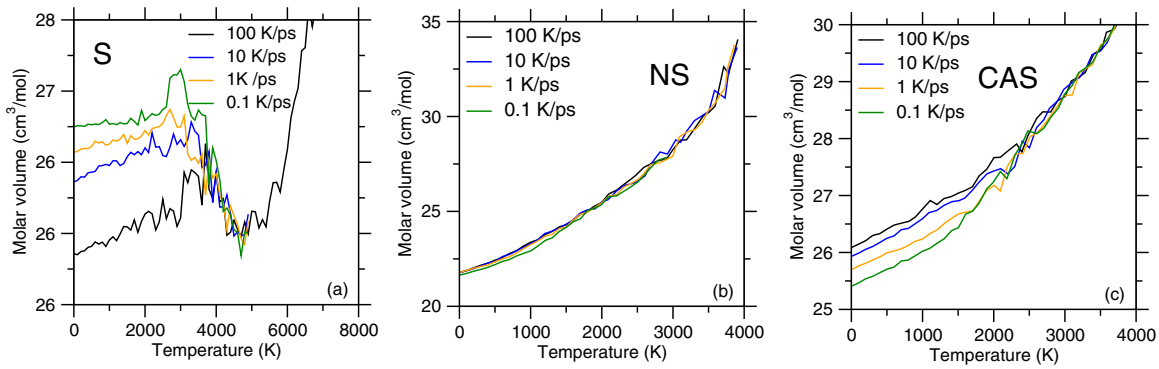

FIG. 2. Molar volume as a function of temperature upon select cooling rates for (a) S, (b) NS, and (c) CAS. Note that each panel has a different y axis.

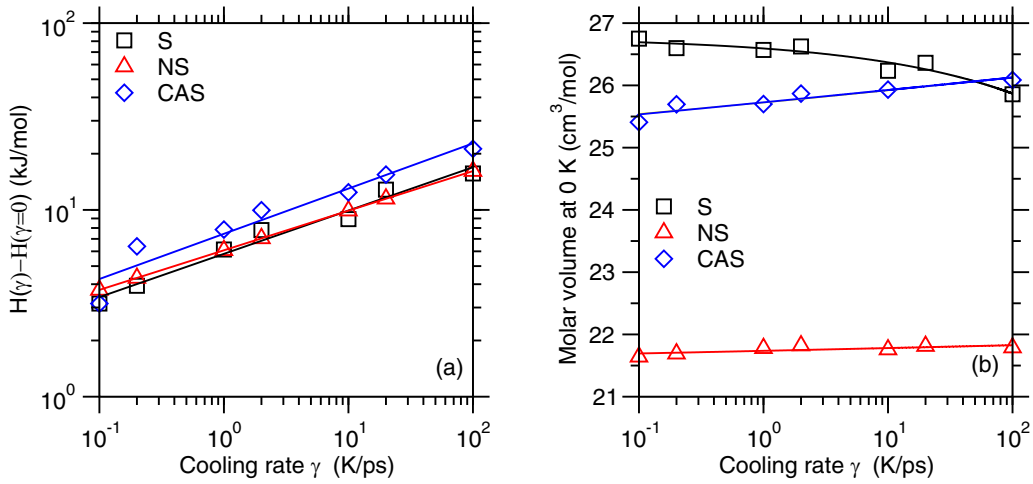

FIG. 3. (a) Residual enthalpy $\Delta H(\gamma) = H(\gamma)$–$H(\gamma = 0)$ at 0 K for the S, NS, and CAS glasses as a function of the cooling rate γ, where $H(\gamma = 0)$ is obtained by fitting $H(\gamma)$ with a power law $H(\gamma) = H(\gamma = 0) + (A\gamma)^{1/\delta}$. The solid lines are power-law fits [see Eq. (1)]. (b) Molar volume at 0 K of the three glasses considered herein as a function of the cooling rate. The solid lines are to guide the eye.

with previous simulations that point to the existence of a liquid-liquid transition in high-temperature liquids and their thermodynamic anomalies [28,54–57]. Note that the location of such transitions might be not be directly comparable to our results because of the sensitivity of such transitions to the employed force field. We note that, once in the glassy state, silica exhibits the lowest extent of thermal expansion, in agreement with experimental results [3]. In general, slower cooling rates result in more compact glasses with lower molar volumes, with the notable exception of silica [58]. NS has the lowest molar volume in general (i.e., more compact), which arises from the fact that Na atoms efficiently fill the empty space within the silicate network [3]. We also note that the cooling rate primarily affects the coefficient of thermal expansion of silica [54], whereas those of the NS and CAS glasses are largely unaffected [17].

B. Effect of the cooling rate on the glass properties

We now turn our attention to the effect of the cooling rate on the glass properties at zero temperature. A log-log plot of the zero-temperature ground-state enthalpy H as a function of the cooling rate γ suggests a power-law dependence, as predicted by mode-coupling theory [17,59]:

$$H(\gamma) = H(\gamma = 0) + (A\gamma)^{1/\delta}, \quad (1)$$

where A and δ are some fitting parameters, and $H(\gamma = 0)$ is the enthalpy that would be achieved for a (fictitious) zero-cooling rate, i.e., after infinitely slow cooling. Note that, in practice, the glass would necessarily crystalize if cooled infinitely slowly [2]. We find $H(\gamma = 0) = -5521$, -3731, and -4711 kJ/mol for S, NS, and CAS, respectively, which scales well with the degree of polymerization (that is, the higher the glass connectivity, the more energetically stable the glass is).

These parameters are used to calculate the residual enthalpy $\Delta H(\gamma) = H(\gamma)$–$H(\gamma = 0)$ of the glass at zero temperature as a function of the cooling rate, that is, the increase in enthalpy at 0 K due to a finite cooling rate γ with respect to the one that would be achieved at zero-cooling rate. As shown in Fig. 3(a), we find that, although the ground-state enthalpy of the three glasses considered herein strongly depends on composition, the dependence on the cooling rate appears to be fairly similar—we find $\delta = 4.3$, 4.7, and 4.1 for the S, NS, and CAS glasses, respectively.

Similarly, we represent in Fig. 3(b) the molar volume at 0 K, which slightly decreases with decreasing cooling rate for NS and CAS glass. Both systems display an opposite behavior to silica, which exhibits an increase in the molar volume with decreasing cooling rate due to its anomalous behavior [18,54]. Overall, we note that the room-temperature molar volume of NS exhibits the lowest dependence on the cooling rate. This likely arises from that, thanks to the high mobility of Na atoms (see Sec. III A and Supplemental Material) [45], the NS glasses are able to partially continue to relax below their fictive temperature—so that the shift of its fictive temperature upon varying cooling rate only has a limited effect on its final volume. This suggests that such low-temperature volume relaxation might not be controlled by the viscosity of the glass [60].

C. Decoupling between enthalpy and volume relaxation

A linear fitting of the high- and low-temperature domains of $H(T)$ or $V_m(T)$ permits one to determine the glass fictive temperature T_f (i.e., as the temperature at which the two linear functions intercept), which, in turn, allows us to substantiate the relationship between T_f and the cooling rate γ (see Fig. 4). In the case of silica, the fictive temperature is defined as the point at which the molar volume starts to decrease with decreasing temperature. As expected, we note that T_f decreases with decreasing cooling rate γ. This arises from the fact that, upon decreasing cooling rate, the threshold at which the relaxation time of the supercooled liquid exceeds the simulation time (i.e., the point at which the system goes out of equilibrium) shifts toward lower temperatures [3]. However, we note that the fictive temperature determined from the break in slope in $V_m(T)$ is systematically higher than that

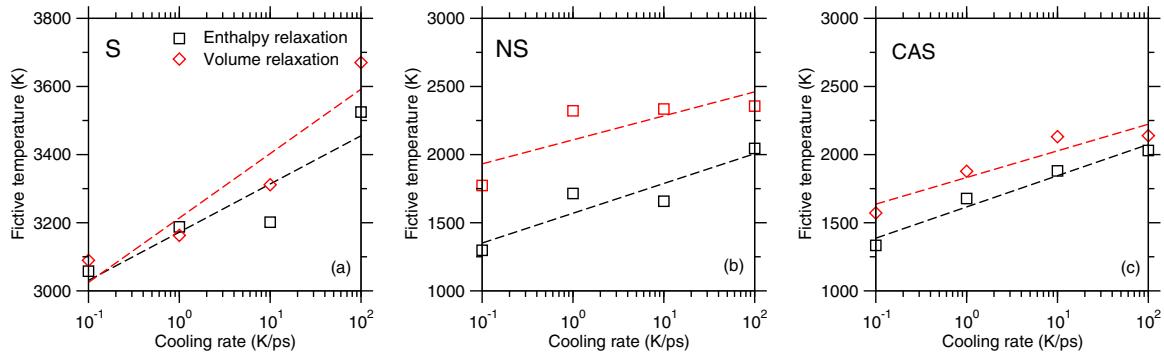

FIG. 4. Fictive temperature T_f as a function of the cooling rate γ for the (a) S, (b) NS, and (c) CAS glasses (calculated from the break in slope of the ground-state enthalpy and molar volume vs temperature curves; see Figs. 1 and 2). The dashed lines are to guide the eye. Note that each panel has a different y axis.

obtained from the break in slope in $H(T)$ (see Fig. 4), which is in line with previous simulations conducted for a Lennard-Jones glass [61]. This suggests the existence of a decoupling between enthalpy and volume relaxation, as further discussed below.

We now further investigate the distinct features of enthalpy and volume relaxation. Although its applicability has been questioned [62–64], the Kissinger equation [65,66] can be conveniently used to estimate the apparent activation energy Δh^* of glass transition or structural relaxation:

$$\ln\left(\frac{\gamma}{T_f^2}\right) = \frac{-\Delta h^*}{RT_f} + \text{const}, \qquad (2)$$

where γ is the cooling rate, T_f the fictive temperature, and R the perfect gas constant. Figure 5 shows the Kissinger plots capturing the dependence of the fictive temperature on the cooling rate for the three glasses considered herein. Overall, we note that, despite the statistical fluctuations that are inherent to small simulated systems, the T_f data can be fairly well fitted by the Kissinger equation—both in the case of enthalpy and volume relaxation. Table I presents the apparent activation energy values resulting for the fits (performed by linear regression of the data presented in Fig. 5). These values are of the same order of magnitude than the apparent activation energy of volume relaxation previously reported for a soda-lime silicate (309 kJ/mol) [66] and a borosilicate glass (615 kJ/mol) [46]. Overall, we observe that the apparent activation energy of silica is significantly larger than those of the sodium silicate and calcium aluminosilicate glasses—both for enthalpy and volume relaxation. This is in line with the fact that the NS and CAS glasses are more depolymerized than silica, which facilitates relaxation.

However, we note that, interestingly, the apparent activation energy associated with volume relaxation is systematically higher than that associated with enthalpy relaxation (by 43% to 65%). This demonstrates the existence of a bifurcation between enthalpy and volume relaxation and suggests they occur via distinct mechanisms. Specifically, our results suggest that volume relaxation is associated with larger energy barriers and, hence, is less kinetically favored than enthalpy relaxation. These observations are in agreement with previous results suggesting that volume relaxation is significantly slower than enthalpy relaxation [60,67]. This was explained from the fact that volume relaxation occurs through long-range reorganizations of the network, whereas enthalpy relaxation occurs through short-range reorganizations [60,68,69].

D. Reversibility of the glass transition

We now focus on the question of the glass reversibility. Once the glasses have been obtained, we heat the systems back up with the same absolute rate as during the cooling protocol (see Sec. II B). Figure 6 represents such

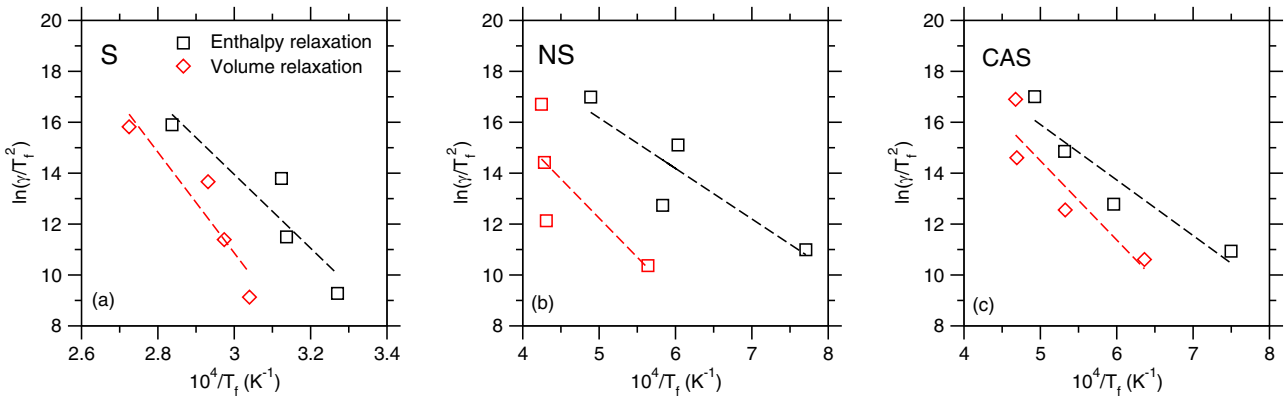

FIG. 5. Kissinger plots for the (a) S, (b) NS, and (c) CAS glasses. The lines are Kissinger fits [Eq. (2)], which allow us to estimate an apparent activation energy of enthalpy and volume relaxation (see Table I).

TABLE I. Apparent activation energies associated to the enthalpy and volume relaxation in the silica, sodium silicate, and calcium aluminosilicate glasses, as obtained by fitting the curves presented in Fig. 5 by Eq. (2).

Glass	Enthalpy relaxation, kJ/mol	Volume relaxation, kJ/mol
Silica (S)	1200	1980
Sodium silicate (NS)	165	239
Calcium aluminosilicate (CAS)	181	259

cooling/heating cycles across the glass transition. We note that, upon reheating, the local ground-state enthalpy differs from that obtained upon cooling, which signals the onset of enthalpic relaxation—as observed experimentally or also evidenced from kinetic constraint models [70]. More specifically, the decrease in the local ground-state enthalpy explored upon reheating indicates that the glass has, indeed, relaxed toward a lower energy state. This feature is compatible with the "overshoot" that is typically observed in calorimetry experiments [71]. However, it is seen that such a behavior is strongly system dependent. For instance, for a given heating/cooling rate (e.g., 1 K/ps), S displays a larger hysteresis curve when compared to the NS or CAS systems.

E. Glass relaxation at the vicinity of the glass transition

In order to further quantify the enthalpy relaxation as a function of temperature, we calculate the enthalpy relaxation $\Delta H = H^{\text{cool}}(T) - H^{\text{heat}}(T)$, which is here defined, at fixed cooling/reheating rate, as the ground-state enthalpy difference between the cooling and the heating curves. Figure 7 represents such quantity for the three systems at different cooling/heating cycles. It is interesting to note that the temperature at which enthalpic relaxation is maximum (i.e., the maximum of ΔH in Fig. 7) is close to the fictive temperature and this typical temperature exhibits qualitatively the same dependence on the cooling rate as that of T_{f}, i.e., it decreases with decreasing cooling rate. This can be understood from the following. At high temperature ($T \gg T_{\text{f}}$), no relaxation is observed since the typical relaxation time is several orders of magnitude lower (picoseconds) than the typical simulation time. As such, the system is at (metastable) equilibrium with no thermodynamic driving force for relaxation. Therefore, the liquid tracks the imposed temperature variation (i.e., $\Delta H = 0$). On the other hand, at low temperature ($T \ll T_{\text{f}}$), relaxation is barely observed because the dynamics is too slow with a large viscosity and relaxation that is kinetically frozen. This is related to the fact that the glass is trapped in some local minimum in the enthalpy landscape [characterized by $H^{\text{cool}}(\gamma)$] and, as a result, the system follows instantaneously the imposed temperature change (i.e., $\Delta H = 0$). Eventually, relaxation can only occur around $T = T_{\text{f}}$, that is, when the relaxation time becomes comparable to the typical observation time.

We further describe the relaxation dynamics by fitting the decrease in enthalpy induced by relaxation with a Gaussian function:

$$\Delta H = \Delta H_{\text{max}} \exp\left[\frac{-(T - T_{\text{max}})^2}{2\Delta T^2}\right], \tag{3}$$

wherein T_{max} represents the temperature where relaxation is maximum, ΔH_{max} the maximum extent of enthalpy relaxation, and ΔT the typical temperature range over which relaxation occurs. Note that $\Delta H(T)$ is not fully symmetric with respect to T_{max} so that a Gaussian function may not offer the best fit (and may not have a clear physical origin). However, the goal of the present fit is only to extract these three relevant fitting parameters. To avoid any spurious effect of the high-temperature fluctuations observed in Fig. 7 on the outcome of the fit, we apply on the data a weighting factor $w = 1/T$ (where T is the temperature) during the fitting procedure. This allows us to place more emphasis on the low-temperature data (which exhibit lower uncertainty). At the highest cooling/heating rate (100 K/ps), we obtain $\Delta H_{\text{max}} = 2.1$, 1.8, and 2.9 kJ/mol for the S, NS, and CAS glasses, respectively. The dependence of the three metrics yielded by the fit on the cooling/heating rate is described in the following (Fig. 8).

For all the glasses considered in the present paper, T_{max} decreases with decreasing cooling/reheating rate [Fig. 8(a)]. The value of T_{max} is very close to the fictive temperature and

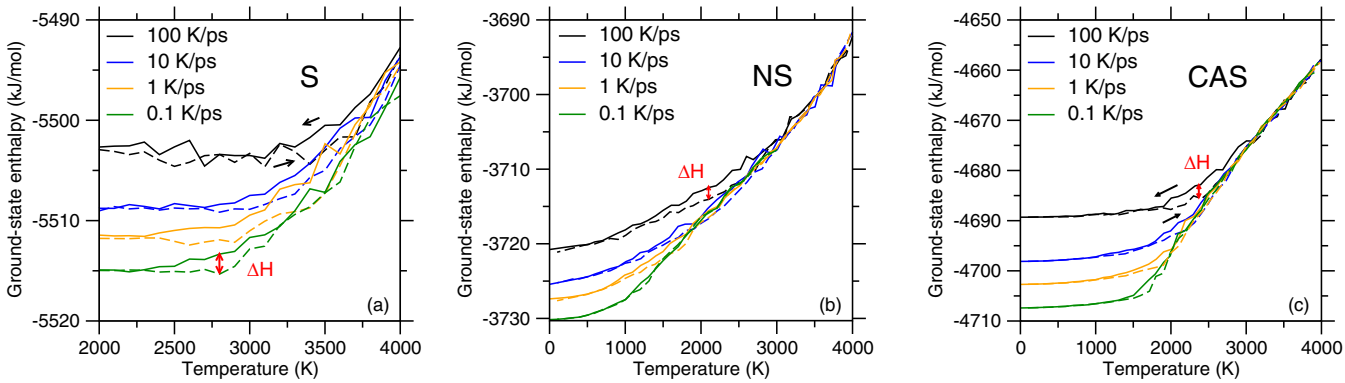

FIG. 6. Local ground-state enthalpy $H(T)$ (i.e., enthalpy of the inherent configuration) as a function of temperature under select cooling/reheating rates for (a) S, (b) NS, and (c) CAS glasses. The solid (same as Fig. 1) and dashed curves refer to the cooling and heating simulations, respectively. Note that each panel has a different y axis.

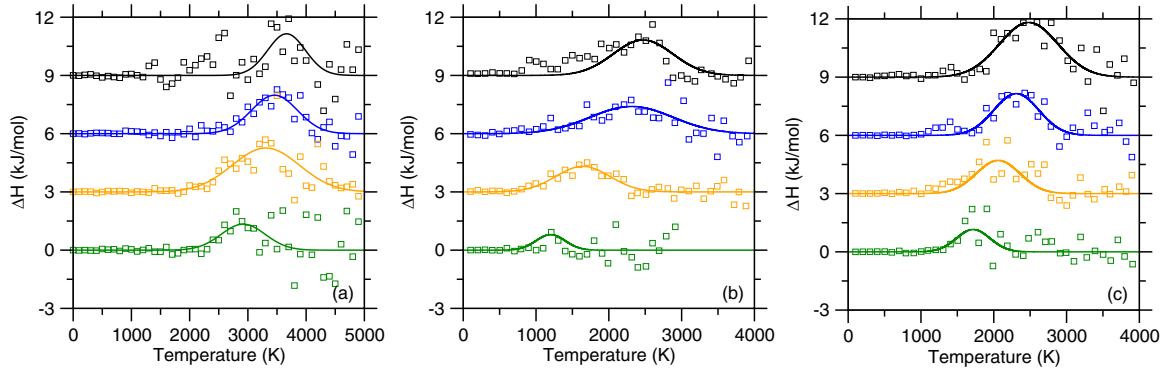

FIG. 7. Relaxation enthalpy (i.e., difference of ground-state enthalpy upon cooling and reheating) as a function of temperature for (a) S, (b) NS, and (c) CAS glasses. The solid lines are Gaussian fits. The values are vertically shifted for clarity. The cooling/reheating rates are (from top to bottom) 100, 10, 1, and 0.1 K/ps.

exhibits a similar dependence on the cooling rate—as also determined recently [72]. We furthermore note that, in the case of the sodium silicate glass, an extrapolation of $T_{\max}(\gamma)$ toward lower cooling rates values (typically 1 K/s) leads to a value that is comparable to the glass transition temperature observed experimentally (see [Ref. [17]]). The $T_{\max}$ of S is overall higher than the $T_{\max}$ of NS and CAS—a result that is also consistent with the experimental observations, i.e., S has the highest T_g, which is reduced once depolymerization is produced by the addition of modifiers as it is the case for NS and CAS [3].

The maximum enthalpy relaxation ($\Delta H_{\max}$) decreases with decreasing cooling rate for the three glasses [Fig. 8(b)]. The origin of this trend is illustrated in Fig. 9 and is explained in the following. Slower cooling rates result in more relaxed (i.e., more stable) glasses [see Figs. 1 and 3(a)]. However, slower heating rates provide more time to the formed glass to further relax upon reheating. Figure 9 shows the typical shape of the stretched-exponential relaxation of a glass in isothermal condition. The black arrows indicate the extent of enthalpy relaxation that can be achieved upon cooling and then reheating. Note that, since the cooling and heating rates are equal to each other, the times over which the system is able to relax at a given temperature upon cooling and subsequent reheating are the same. However, due to the stretched-exponential nature of glass relaxation, the extent of relaxation achieved upon reheating is lower than that achieved upon cooling. The red arrows now indicate the relaxation that can be achieved upon slower cooling and reheating. It can be observed that, although the observation (simulation) time increases, the actual extent of enthalpy relaxation is lower than upon faster cooling/reheating. As such, varying the cooling/heating rate can be used to describe the relaxation dynamics at different stages, namely, early-stage relaxation for high cooling/heating rates and longer-term relaxation for lower cooling/heating rates (see Fig. 9). Hence, the fact that $\Delta H_{\max}$ decreases with decreasing cooling/heating rate indicates that most of the relaxation occurs at early stage and that the relaxation dynamics subsequently slows down, consistently with the stretched-exponential nature of glass relaxation) [15,60,67,68,73,74]. Overall, we find that NS has the smallest $\Delta H_{\max}$. This may arise from the high mobility of the Na atoms, which allows some significant relaxation to occur during the cooling phase at $T < T_f$.

Finally, we focus our attention on ΔT [see Fig. 8(c)]. ΔT can be considered as being the extent of temperature over which relaxation can occur, that is, over which the relaxation time of the glass is high enough (i.e., otherwise the system

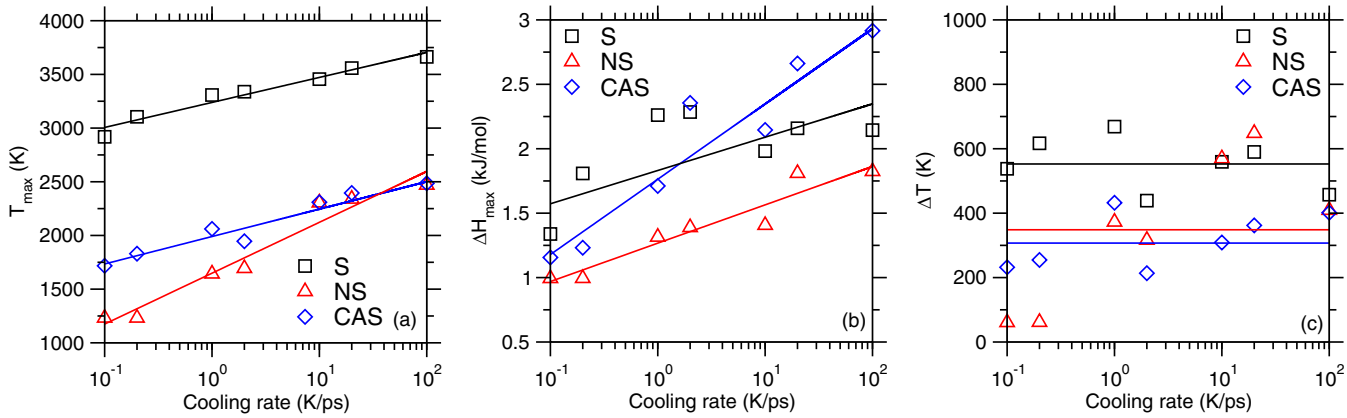

FIG. 8. (a) Temperature at which the enthalpy relaxation is maximum ($T_{\max}$), (b) maximum extent of enthalpy relaxation ($\Delta H_{\max}$), and (c) typical range of temperature over which enthalpy relaxation occurs (ΔT) as a function of the cooling/heating rate for S, NS, and CAS. The lines are to guide the eye.

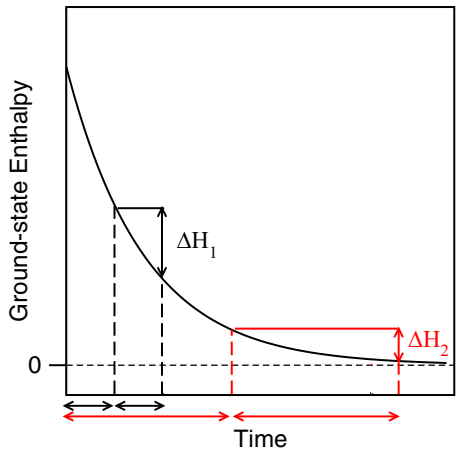

FIG. 9. Schematic showing the typical stretched-exponential enthalpy relaxation of a glass in isothermal conditions. The arrows indicate the extent of relaxation that can be achieved between cooling and subsequent reheating in the case of (black) fast cooling/heating and (red) slow cooling/heating.

would have already fully relaxed upon cooling and would be at equilibrium), but not too high (i.e., otherwise relaxation would be too slow to be observed at all within the timescale of our simulation)—i.e., ΔT is the range of temperature for which the relaxation time is high enough for the system to be out of equilibrium, but low enough for relaxation to be kinetically allowed. Hence, relaxation is only observed when the relaxation time of the glass becomes comparable to that of our simulation time. Based on this, the extent of temperature over which the relaxation time is comparable to the simulation time should be controlled by the derivative of the relaxation time with respect to temperature (i.e., the glass fragility) [75]. Since the viscosity (and relaxation time) increases exponentially with decreasing temperature, we would expect, upon decreasing cooling rate, the extent of the temperature window over which the relaxation time is comparable to the simulation time should decrease. This should result in a more well-defined glass transition (i.e., lower ΔT) upon decreasing cooling rate. Although such a trend is partially verified for the NS and CAS glasses [see Fig. 8(c)], the fluctuations in the data do not allow us to conclusively confirm this behavior. The relationship between ΔT and glass fragility is also in agreement with the fact that we find silica to exhibit the largest ΔT, in agreement with its low fragility value [76].

IV. CONCLUSIONS

In summary, we have studied relaxation and glass transition reversibility in three archetypical silicate glasses by means of molecular dynamics simulations. Overall, the simulations reproduce the generic features of the glass transition and of its dependence on the cooling rate. This analysis confirms that the glass ground-state enthalpy (i.e., the position locally occupied by the glass within the enthalpy landscape) exhibits a power-law dependence on the cooling rate, in agreement with mode-coupling theory. Based on these simulations, a systematic bifurcation between enthalpy and volume relaxation is evidenced, which suggests that they occur via distinct mechanisms. Finally, based on a methodology combining thermal cycles and inherent configuration analysis, we characterize the degree of (ir)reversibility of the glass transition. We find that both the extent of irreversibility and the range of temperature over which relaxation occurs are strongly system-specific. Overall, the present results provide a numerical assessment of the calorimetric glass transition using MD simulations, and should permit investigation in the future of the effect of composition or pressure on glass relaxation.

ACKNOWLEDGMENTS

This work was supported by the National Science Foundation under Grants No. 1562066, No. 1762292, and No. 1826420, and by Corning Incorporated through the Glass Age Scholarship.

[1] P. G. Debenedetti and F. H. Stillinger, Nature (London) **410**, 259 (2001).
[2] E. D. Zanotto and J. C. Mauro, J. Non-Cryst. Solids **471**, 490 (2017).
[3] A. K. Varshneya, *Fundamentals of Inorganic Glasses* (Academic, San Diego, 1993).
[4] M. M. Smedskjaer, M. Bauchy, J. C. Mauro, S. J. Rzoska, and M. Bockowski, J. Chem. Phys. **143**, 164505 (2015).
[5] M. Wang, B. Wang, T. K. Bechgaard, J. C. Mauro, S. J. Rzoska, M. Bockowski, M. M. Smedskjaer, and M. Bauchy, J. Non-Cryst. Solids **454**, 46 (2016).
[6] O. Gulbiten, J. C. Mauro, X. Guo, and O. N. Boratav, J. Am. Ceram. Soc. **101**, 5 (2017).
[7] Y.-Z. Yue, J. Non-Cryst. Solids **354**, 1112 (2008).
[8] J. Jackle, Rep. Prog. Phys. **49**, 171 (1986).
[9] A. Ellison and I. A. Cornejo, Int. J. Appl. Glass Sci. **1**, 87 (2010).
[10] M. Bauchy and M. Micoulaut, Nat. Commun. **6**, 6398 (2015).
[11] B. Mantisi, M. Bauchy, and M. Micoulaut, Phys. Rev. B **92**, 134201 (2015).
[12] Edited by C. Massobrio, J. Du, M. Bernasconi, and P. S. Salmon, *Molecular Dynamics Simulations of Disordered Materials* (Springer International, Cham, 2015).
[13] C. Yildirim, J.-Y. Raty, and M. Micoulaut, J. Chem. Phys. **144**, 224503 (2016).
[14] P. Boolchand and B. Goodman, MRS Bull. **42**, 23 (2017).
[15] M. Micoulaut, Rep. Prog. Phys. **79**, 066504 (2016).
[16] J. Du, in *Molecular Dynamics Simulations of Disordered Materials*, edited by C. Massobrio, J. Du, M. Bernasconi, and P. S. Salmon (Springer International, Cham, 2015), pp. 157–180.
[17] X. Li, W. Song, K. Yang, N. M. A. Krishnan, B. Wang, M. M. Smedskjaer, J. C. Mauro, G. Sant, M. Balonis, and M. Bauchy, J. Chem. Phys. **147**, 074501 (2017).
[18] K. Vollmayr, W. Kob, and K. Binder, Phys. Rev. B **54**, 15808 (1996).
[19] Y. Guissani and B. Guillot, J. Chem. Phys. **98**, 8221 (1993).

[20] M. Bauchy, B. Guillot, M. Micoulaut, and N. Sator, Chem. Geol. **346**, 47 (2013).

[21] R. C. Welch, J. R. Smith, M. Potuzak, X. Guo, B. F. Bowden, T. J. Kiczenski, D. C. Allan, E. A. King, A. J. Ellison, and J. C. Mauro, Phys. Rev. Lett. **110**, 265901 (2013).

[22] J. C. Mauro, A. J. Ellison, and L. D. Pye, Int. J. Appl. Glass Sci. **4**, 64 (2013).

[23] S. Plimpton, J. Comput. Phys. **117**, 1 (1995).

[24] S. Nosé, Mol. Phys. **52**, 255 (1984).

[25] W. G. Hoover, Phys. Rev. A **31**, 1695 (1985).

[26] B. W. H. van Beest, G. J. Kramer, and R. A. van Santen, Phys. Rev. Lett. **64**, 1955 (1990).

[27] F. Yuan and L. Huang, Sci. Rep. **4**, 5035 (2014).

[28] J. Horbach and W. Kob, Phys. Rev. B **60**, 3169 (1999).

[29] B. Wang, Y. Yu, Y. J. Lee, and M. Bauchy, Front. Mater. **2**, 1 (2015).

[30] Y. Yu, B. Wang, M. Wang, G. Sant, and M. Bauchy, J. Non-Cryst. Solids **443**, 148 (2016).

[31] J. Du and A. N. Cormack, J. Non-Cryst. Solids **349**, 66 (2004).

[32] M. Bauchy, J. Chem. Phys. **137**, 044510 (2012).

[33] J. Du and L. R. Corrales, Phys. Rev. B **72**, 092201 (2005).

[34] A. Pedone, G. Malavasi, A. N. Cormack, U. Segre, and M. C. Menziani, Chem. Mater. **19**, 3144 (2007).

[35] Y. Yu, B. Wang, Y. J. Lee, and M. Bauchy, *MRS Online Proceedings Library Archive*, Vol. 1757 (MRS, Warrendale, 2015).

[36] M. Bauchy, B. Wang, M. Wang, Y. Yu, M. J. Abdolhosseini Qomi, M. M. Smedskjaer, C. Bichara, F.-J. Ulm, and R. Pellenq, Acta Mater. **121**, 234 (2016).

[37] M. Bauchy and M. Micoulaut, EPL Europhys. Lett. **104**, 56002 (2013).

[38] B. Wang, Y. Yu, M. Wang, J. C. Mauro, and M. Bauchy, Phys. Rev. B **93**, 064202 (2016).

[39] M. Micoulaut and M. Bauchy, Phys. Rev. Lett. **118**, 145502 (2017).

[40] M. Bouhadja, N. Jakse, and A. Pasturel, J. Chem. Phys. **138**, 224510 (2013).

[41] N. Jakse, M. Bouhadja, J. Kozaily, J. W. E. Drewitt, L. Hennet, D. R. Neuville, H. E. Fischer, V. Cristiglio, and A. Pasturel, Appl. Phys. Lett. **101**, 201903 (2012).

[42] M. Bauchy, J. Chem. Phys. **141**, 024507 (2014).

[43] T. K. Bechgaard, O. Gulbiten, J. C. Mauro, Y. Hu, M. Bauchy, and M. M. Smedskjaer, Am. Ceram. Soc. Bull. **97**, 31 (2018).

[44] N. M. A. Krishnan, B. Wang, Y. Yu, Y. Le Pape, G. Sant, and M. Bauchy, Phys. Rev. X **7**, 031019 (2017).

[45] See Supplemental Material at http://link.aps.org/supplemental/10.1103/PhysRevB.98.104205 for more details about the molecular dynamics simulations conducted herein.

[46] C. T. Moynihan, A. J. Easteal, M. A. De Bolt, and J. Tucker, J. Am. Ceram. Soc. **59**, 12 (1976).

[47] A. Agarwal, K. M. Davis, and M. Tomozawa, J. Non-Cryst. Solids **185**, 191 (1995).

[48] A. Agarwal and M. Tomozawa, J. Am. Ceram. Soc. **78**, 827 (2005).

[49] J. F. Stebbins, E. V. Dubinsky, K. Kanehashi, and K. E. Kelsey, Geochim. Cosmochim. Acta **72**, 910 (2008).

[50] N. Giovambattista, C. A. Angell, F. Sciortino, and H. E. Stanley, Phys. Rev. E **72**, 011203 (2005).

[51] M. Bauchy and M. Micoulaut, Phys. Rev. B **83**, 184118 (2011).

[52] J. C. Mauro and M. M. Smedskjaer, J. Non-Cryst. Solids **396–397**, 41 (2014).

[53] A. Q. Tool, J. Am. Ceram. Soc. **29**, 240 (1946).

[54] J. M. D. Lane, Phys. Rev. E **92**, 012320 (2015).

[55] J. L. Barrat, J. Badro, and P. Gillet, Mol. Simul. **20**, 17 (1997).

[56] M. Micoulaut, Chem. Geol. **213**, 197 (2004).

[57] M. S. Shell, P. G. Debenedetti, and A. Z. Panagiotopoulos, Phys. Rev. E **66**, 011202 (2002).

[58] R. Brückner, J. Non-Cryst. Solids **5**, 123 (1970).

[59] W. Kob and H. C. Andersen, Phys. Rev. E **51**, 4626 (1995).

[60] Y. Yu, M. Wang, M. M. Smedskjaer, J. C. Mauro, G. Sant, and M. Bauchy, Phys. Rev. Lett. **119**, 095501 (2017).

[61] K. Vollmayr, W. Kob, and K. Binder, J. Chem. Phys. **105**, 4714 (1996).

[62] R. Svoboda, J. Therm. Anal. Calorim. **118**, 1721 (2014).

[63] R. L. Blaine and H. E. Kissinger, Thermochim. Acta **540**, 1 (2012).

[64] R. Svoboda, P. Čičmanec, and J. Málek, J. Therm. Anal. Calorim. **114**, 285 (2013).

[65] H. E. Kissinger, Anal. Chem. **29**, 1702 (1957).

[66] O. S. Narayanaswamy, J. Am. Ceram. Soc. **54**, 491 (1971).

[67] Y. Yu, M. Wang, D. Zhang, B. Wang, G. Sant, and M. Bauchy, Phys. Rev. Lett. **115**, 165901 (2015).

[68] M. Potuzak, R. C. Welch, and J. C. Mauro, J. Chem. Phys. **135**, 214502 (2011).

[69] N. M. A. Krishnan, B. Wang, Y. Le Pape, G. Sant, and M. Bauchy, Phys. Rev. Mater. **1**, 053405 (2017).

[70] M. Micoulaut, J. Phys.: Condens. Matter **22**, 285101 (2010).

[71] P. Badrinarayanan, W. Zheng, Q. Li, and S. L. Simon, J. Non-Cryst. Solids **353**, 2603 (2007).

[72] D. S. Sanditov and M. I. Ojovan, Phys. B Condens. Matter **523**, 96 (2017).

[73] Y. Yu, J. C. Mauro, and M. Bauchy, Am. Ceram. Soc. Bull. **96**, 34 (2017).

[74] J. C. Phillips, Rep. Prog. Phys. **59**, 1133 (1996).

[75] C. A. Angell *et al.*, Science **267**, 1924 (1995).

[76] R. Böhmer, K. L. Ngai, C. A. Angell, and D. J. Plazek, J. Chem. Phys. **99**, 4201 (1998).